Bio-Design and Manufacturing (2024) 7:388–398
https://doi.org/10.1007/s42242-024-00278-2

RESEARCH ARTICLE

Flexible, high-density, laminated ECoG electrode array for high spatiotemporal resolution foci diagnostic localization of refractory epilepsy

Yafeng Liu[1,2,3] · Zhouheng Wang[1,2] · Yang Jiao[1,2] · Ying Chen[4,5] · Guangyuan Xu[1,2,6] · Yinji Ma[1,2] · Xue Feng[1,2]

Received: 13 June 2023 / Accepted: 1 April 2024 / Published online: 17 June 2024

Abstract

High spatiotemporal resolution brain electrical signals are critical for basic neuroscience research and high-precision focus diagnostic localization, as the spatial scale of some pathologic signals is at the submillimeter or micrometer level. This entails connecting hundreds or thousands of electrode wires on a limited surface. This study reported a class of flexible, ultrathin, high-density electrocorticogram (ECoG) electrode arrays. The challenge of a large number of wiring arrangements was overcome by a laminated structure design and processing technology improvement. The flexible, ultrathin, high-density ECoG electrode array was conformably attached to the cortex for reliable, high spatial resolution electrophysiologic recordings. The minimum spacing between electrodes was 15 μm, comparable to the diameter of a single neuron. Eight hundred electrodes were prepared with an electrode density of 4444 mm^{-2}. In focal epilepsy surgery, the flexible, high-density, laminated ECoG electrode array with 36 electrodes was applied to collect epileptic spike waves in rabbits, improving the positioning accuracy of epilepsy lesions from the centimeter to the submillimeter level. The flexible, high-density, laminated ECoG electrode array has potential clinical applications in intractable epilepsy and other neurologic diseases requiring high-precision electroencephalogram acquisition.

Keywords Electrocorticogram (ECoG) electrode · Epilepsy · High density · High resolution · Laminated structure

Introduction

Research on brain–computer interface (BCI) systems in recent decades for clinical treatment or communication of patients with major diseases, such as epilepsy and severe paralysis, has increased significantly [1, 2]. BCI systems detect epileptic spike waves to identify epileptogenic zones [3, 4]. Epileptic spike waves are generated by the high-frequency repetitive discharge of the epileptic focus cell group related to the abnormal discharge of spatially highly localized neurons [5]. The electrocorticogram (ECoG) is a good source signal to balance surgical injury and signal accuracy, especially for the clinical BCI system of epileptic patients [6–10]. However, 40% to 50% of patients have poor surgical outcomes, which is caused by an inaccurate localization of the epileptic focus due to the electrode size of standard ECoG electrodes being too large [5, 11–13]. In addition, a mechanical mismatch between ECoG electrodes and tissues is likely to elicit an inflammatory tissue response, leading to the proliferation of a glial cell sheath, which hinders the acquisition of action potentials [14].

In the past decade, flexible electronic technology has made great progress [15–22]. Compared to traditional equipment, devices based on flexible electronic technology establish a stable interface with tissues due to the advantages of an ultrathin, soft, lightweight, and deformable

✉ Yinji Ma
mayinji@mail.tsinghua.edu.cn

✉ Xue Feng
fengxue@tsinghua.edu.cn

1 Applied Mechanics Laboratory, Department of Engineering Mechanics, Tsinghua University, Beijing 100084, China

2 Laboratory of Flexible Electronics Technology, Tsinghua University, Beijing 100084, China

3 College of Artificial Intelligence, Southwest University, Chongqing 400715, China

4 Institute of Flexible Electronics Technology of THU, Jiaxing 314000, China

5 Qiantang Science and Technology Innovation Center, Hangzhou 310016, China

6 School of Artificial Intelligence, Beijing University of Posts and Telecommunications, Beijing 100876, China

structure that will not cause discomfort or allergic reactions [23–26]. ECoG electrodes based on flexible electronic technology can eliminate the mechanical mismatch between the electrode and brain tissue properties [27], thereby minimizing the risks of infection and inflammation [28]. Its shape adaptability enables the device to adapt to the complex shape and irregular structure of the brain's superficial sulcus and gyrus, enabling good contact and nonslip between the electrode and the cortex to record high-quality cortical electroencephalograms (EEGs) [29–31].

High spatiotemporal resolution brain electrical signals are critical for basic neuroscience research and high-precision focus diagnostic localization, as the spatial scale of some pathologic signals is at the submillimeter or micrometer level. Higher-density electrodes will enable collected brain signals with more details, which is significant for understanding brain function mechanisms and clinical applications [8, 32]. However, the high-resolution ECoG interface is difficult to develop due to the inability to connect hundreds or thousands of wires in a narrow area [33–36]. The challenges of a large number of wiring arrangements and the related manufacturing technology of high-density electrodes are crucial for high-density brain electrode arrays [34, 35, 37]. Meanwhile, high-density electrodes generally have a smaller contact area with tissues, leading to higher interface impedance and lower signal quality [38–41]. Therefore, it is still a challenge to design an ECoG array that meets the requirements of high density, low impedance, and flexibility.

This study reported a class of flexible, high-density, laminated ECoG electrode arrays that can effectively record high-resolution ECoG. First, this study reported the manufacture of an ultrathin, high-density ECoG electrode array with laminated structure to achieve high spatiotemporal resolution electrical recordings from cortical regions. The laminated structure design enabled the electrode leads to be located in different spatial positions, overcoming the challenges of a large number of wiring arrangements. In the preparation process, a tempering process was introduced to eliminate the residual thermal stress inside the laminated film structure and overcome the cracking problem of flexible, high-density, laminated ECoG electrodes. In the advanced application of focal epilepsy surgery, the flexible, ultrathin, high-density ECoG electrode introduced in this study can realize the submillimeter-level high-resolution positioning of epileptic lesions and has potential clinical applications in intractable epilepsy and other neurologic diseases requiring high-precision EEG acquisition.

Results and discussion

To achieve high-resolution neuroelectric signal acquisition, a flexible, ultrathin, high-density, laminated ECoG electrode array was developed using flexible electronic technology. Flexible, high-density, laminated ECoG electrodes consisted of four parts: a polyimide (PI) cover, laminated aligned electrodes, a dielectric layer, and a PI base (Fig. 1a). Polymethyl methacrylate (PMMA) was prepared on a silicon wafer by spin-coating. A PI film as the support layer was spin-coated over PMMA and cured. Tempering was performed at 250 °C for 1 h. The Cr/Au layers were deposited and photolithographed into a pattern array. The dielectric layer was fabricated by spin-coating PI over the designed mesh patterns. The previous steps were repeated, ensuring that the first- and second-layer electrode arrays were staggered in space. The front and back sides of the multilayer PI/Au film were etched to the electrode and connector pad, respectively, by reactive ion etching (RIE) masked by Cu. Flexible, high-density, laminated ECoG electrodes were obtained after peeling them off. An ultra-large number of space-staggered multilayer electrode arrays were fabricated by repeating the above steps.

The electrode size is related to electrode capacitance and impedance. A larger electrode size corresponds to larger electrode capacitance and smaller electrode impedance, which can prevent electrode polarization and ensure the stability of EEG signal acquisition. Meanwhile, a smaller electrode size is the key to achieving high-density electrodes. The size of one neuron is usually >10 μm [42, 43]. A balance needs to be made among electrode density, impedance, and capacitance. Therefore, the electrode size is generally not smaller than 10 μm. In Fig. 1b, the minimum interelectrode spacing is only 15 μm, comparable to the size of a single neuron (<50 μm). The challenges of a large number of wiring arrangements and the related manufacturing technology of the high-density flexible ECoG electrodes worldwide are overcome by a laminated structure design and processing technology improvement. The electrode arrays in different layers are staggered and will not overlap. The number of electrodes in the flexible ECoG electrode array with four laminated layers was 800, much higher than that of the 256-channel NeuroGrid [35]. Moreover, the flexible laminated electrode array is scalable, and its channels can be increased according to the number of laminated layers. The density of the flexible ECoG electrode array was 4444 electrodes per mm^2, four times higher than the reported highest density of the NeuroGrid (interelectrode spacing 30 μm, electrode density is approximately 1000 electrodes per mm^2) in the world. The density of the flexible, high-density ECoG electrode array can be further increased by the laminated structure if necessary.

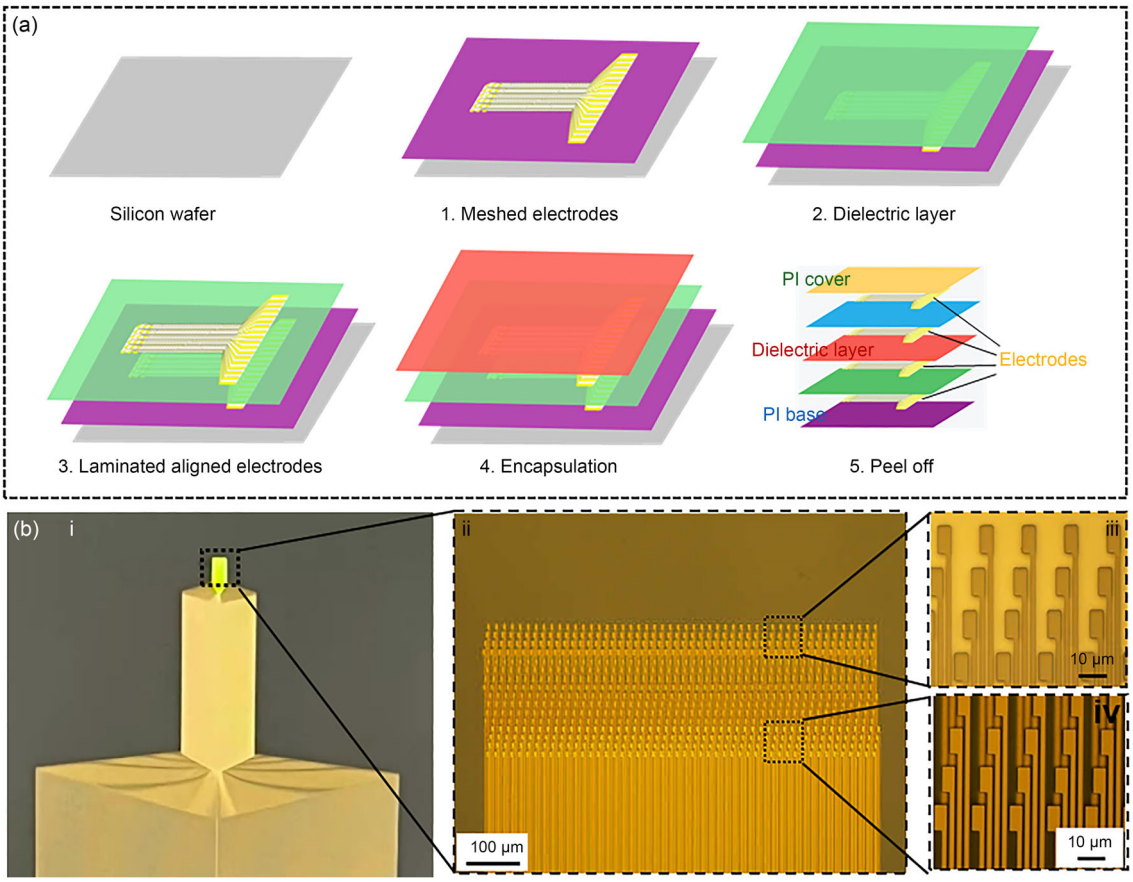

Fig. 1 **a** Schematic diagram of flexible, high-density, laminated ECoG electrode preparation; **b** high-density, laminated ECoG electrode array with a minimum interelectrode spacing of 15 μm and a total number of electrodes of 800. ECoG: electrocorticogram; PI: polyimide

The optimization value of electrode spacing was analyzed by Freeman et al. [39]. The optimized value of electrode spacing was about 1 mm based on the spatial spectrum analysis [39, 44]. To study the localization of the epileptic focus, a flexible, high-density, laminated ECoG electrode with a two-layer electrode structure was developed, and the electrode spacing was 1 mm. The size of the flexible, high-density, laminated ECoG electrode array was designed to be just enough to cover the rabbit cortex. In Fig. 2a, the flexible, high-density, laminated ECoG electrode array is a PI-based round-dot electrode with 36 channels (6×6 patches) and an overall width of 10 mm. The monolayer electrode array has 18 channels (3×6 patches; Fig. S1 in Supplementary Information). The top layer of the electrode array is covered with a PI layer. Additional polymeric encapsulation layers prevent electrical leakage currents when the flexible, high-density, laminated ECoG electrode is immersed in the rabbit brain.

The electrode array in different layers is staggered and does not overlap (Fig. 2b). The flexible, high-density, laminated ECoG electrode array is very soft and can be easily and conformably attached to uneven surfaces (Fig. 2c), enabling steady contact between the electrode and tissues. The flexible, high-density, laminated ECoG electrode array adheres to the human skin through van der Waals forces. The cerebral cortex is a wet environment. The flexible, high-density, laminated ECoG electrode array can achieve conformal attachment through tissue fluid with strong interface energy, which can be validated similarly to the cortical tissue (Fig. S2 in Supplementary Information). Meanwhile, ECoG electrodes based on flexible electronic technology can eliminate the mechanical mismatch between the electrode and brain tissue properties, thereby minimizing the risks of infection and inflammation. In Fig. 2d, the width of the gold wire is 100 μm. The recording area of each channel is 0.785 mm^2 (circle with a diameter of 1 mm). The larger contact area ensures a lower interface impedance between the electrode and the cortical surface, which helps improve the signal-to-noise ratio (SNR). The morphology of the electrode is complete, indicating that it has excellent mechanical and electrical properties.

The tempering process in the curing process of PI is critical. During the curing process, residual stress is generated inside the PI layer, which is generated by the freezing of the directional conformation of macromolecular chains and uneven shrinkage during cooling. Furthermore, the difference in curing times varies the thermal expansion coefficients

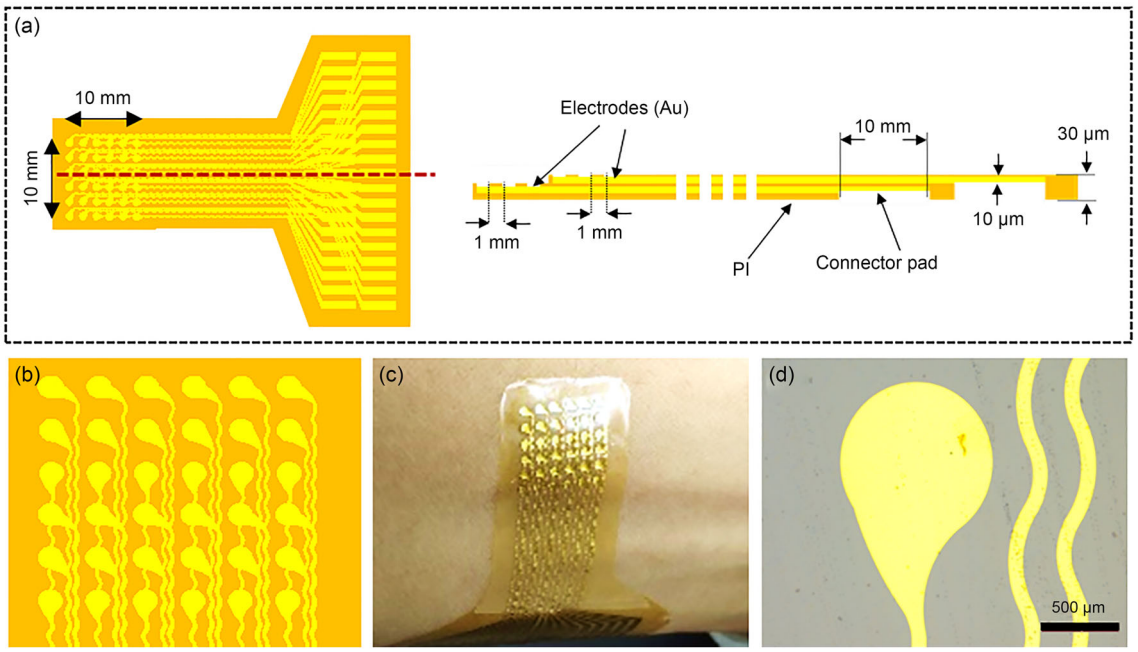

Fig. 2 **a** Plain and side views of flexible, high-density, laminated ECoG electrodes with an interelectrode spacing of 2 mm and a total channel of 36; **b** enlarged view of the contact structure; **c** flexible, high-density, laminated ECoG electrodes conformably attached to the uneven skin surface of humans; **d** enlarged view of flexible, high-density, laminated ECoG electrodes. ECoG: electrocorticogram

of laminated PI layers resulting in residual stress between layers. The superposition of residual stresses within and between layers would cause crack initiation and propagation in the PI layers of the flexible, high-density, laminated ECoG electrode array. The tempering process would accelerate the relaxation of PI. The relaxation time of polymers would be shortened at high temperatures, which could eliminate internal residual thermal stress, reduce the stress mismatch of PI between different layers, and prevent cracks from being generated inside the PI film (Fig. S3 in Supplementary Information).

In Fig. 3a, the bending radii of the electrodes are 5, 2, and 1 cm. With a decrease in the bending radius, the strain of the electrode increases. The maximum strain is approximately 0.07%, far less than the ductility limit of gold. The extreme flexibility of the device, which was approximately 30 μm thick, allowed it to be folded (Fig. 3b), allowing conformal attachment to the uneven surface of the cerebral cortex. This can improve the stability of the interface impedance between the electrode and the cerebral cortex and reduce the drift of the ECoG signal. The electrochemical properties of the flexible, high-density, laminated ECoG electrode array were also characterized (Fig. 3c). The mean charge measured before (0.15 μC) and after (0.14 μC) bending was not significantly different. The charge storage of the flexible, high-density ECoG electrode (0.785 mm^2; capacity 0.19 $\mu C/mm^2$) was comparable to previous values, and the charge storage values before and after bending (0.19 and 0.17 $\mu C/mm^2$) did not change significantly [45–47]. Low electrode impedance of the electrode array is the key to obtaining high-quality ECoG signals. In Fig. 3d, electrochemical impedance spectroscopy of the flexible, high-density, laminated ECoG electrode array was performed. The impedance magnitude at 1 kHz was only 5.3 kΩ, much smaller than the previous result (approximately 27 kΩ) [30]. The impedance at 1 kHz was not significantly different before (5.3 kΩ) or after (6.5 kΩ) bending, indicating that the flexible, high-density, laminated ECoG electrode array has good SNR and impedance stability.

In addition, the fidelity of collected bioelectric signals is an important indicator for evaluating electrode performance. A square wave with a frequency of 30 Hz was generated by a signal generator to propagate the signal in phosphate-buffered saline (PBS) buffer (simulated tissue fluid). The flexible, high-density, laminated ECoG electrode array was put into a PBS buffer to collect the signal. In Fig. 3e, the peak amplitudes of the periodic signal in the simulated source were measured using the flexible, high-density, laminated ECoG electrode array. The signal amplitudes collected by electrodes were all kept within the range of −0.2 to 0.2 μV. The square-wave signal was completely restored with an accurate phase. The characteristic frequency of the collected signal was 30 Hz (Fig. 3f), consistent with the frequency of the transmitted signal, indicating that the electrode can accurately record the

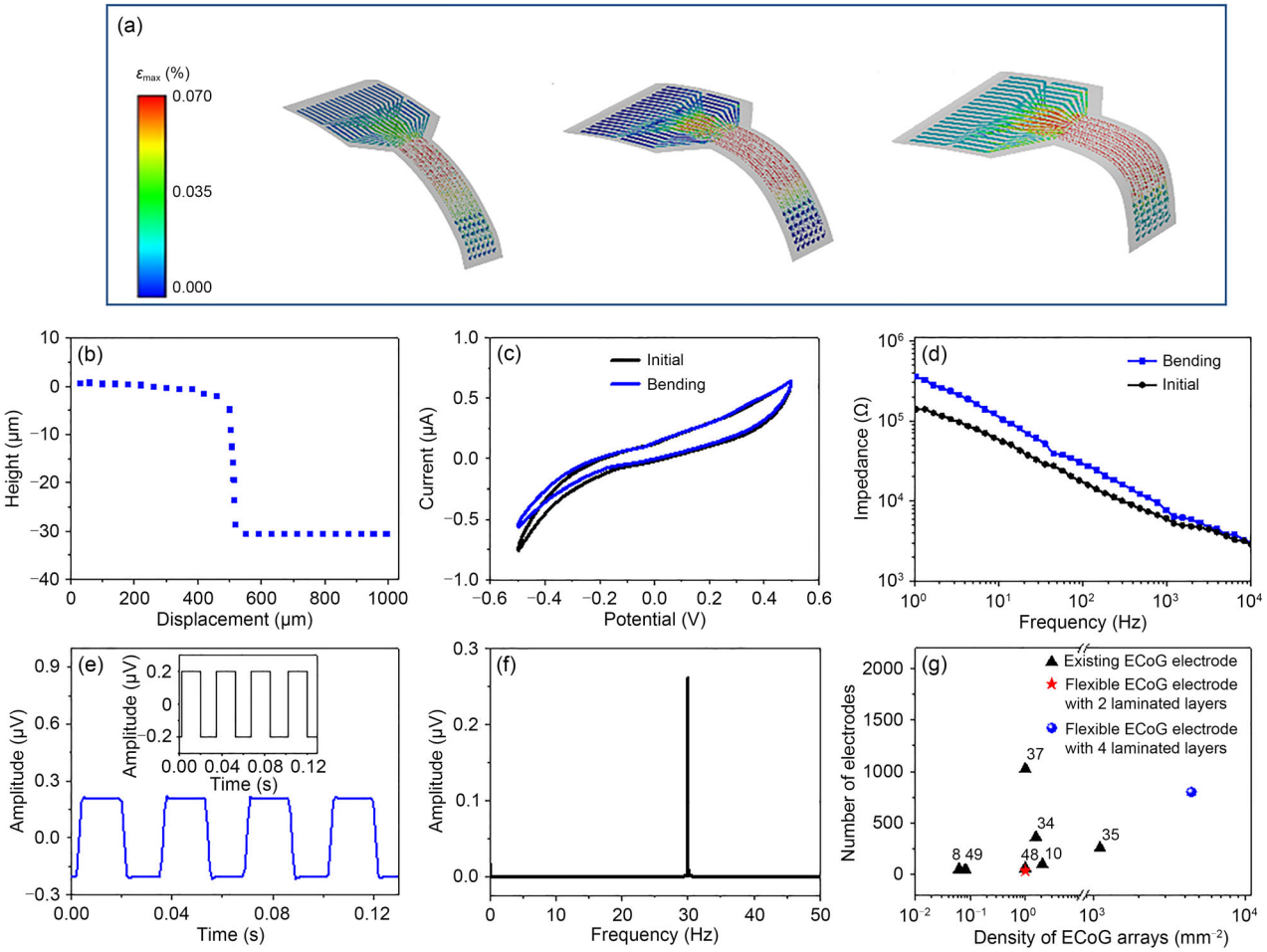

Fig. 3 **a** Strain of the flexible, high-density, laminated ECoG electrode array under different bending radii simulated by finite-element analysis. **b** Thickness (30 μm) of the flexible, high-density, laminated ECoG electrode. **c** Voltage–ampere curve. **d** Impedance spectrum. **e** Simulation of bioelectric signal acquisition. **f** Signal spectrum analysis. **g** Comparison of electrode density [8, 10, 34, 35, 37, 48, 49]. ECoG: electrocorticogram

frequency range of the signal, which is crucial for ECoG signal acquisition.

In Fig. 3g and Table S1 (Supplementary Information), the density of the flexible ECoG electrode array with four laminated layers is 4444 per mm^2, four times higher than the reported highest density of the NeuroGrid (interelectrode spacing of 30 μm, electrode density of approximately 1000 electrodes per mm^2, with 256 electrodes) in the world [35]. The flexible, high-density, laminated ECoG electrode array with two laminated layers also increased the electrode density by 100 times compared to the standard ECoG, which ensured the main advantage of more intensive spatial sampling. The overall thickness of the resultant device is highly relevant to the flexibility and conformability of the flexible, high-density, laminated ECoG electrode. The flexural rigidity (I) of a flexible, high-density, laminated ECoG electrode array should be less than cerebral cortex. The flexural rigidity can be expressed as $EI=Ebh^3/12$, where h is the thickness, b is the width of the resultant device, and E is the elastic modulus. Therefore, it can be expressed as

$$E_{\mathrm{PI}}h_{\mathrm{PI}}^3 \le E_{\mathrm{cortex}}h_{\mathrm{cortex}}^3.$$

Here, $h_{\mathrm{cortex}} \le 4.5$ mm [50], $E_{\mathrm{cortex}} \le 10$ kPa [51, 52], and $E_{\mathrm{PI}} \approx 300$ MPa. The thickness of the flexible, high-density, laminated ECoG electrode array is calculated as $h_{\mathrm{PI}} \le 67.2$ μm. Therefore, the overall thickness of the resultant device should be <67.2 μm. The thickness of the flexible ECoG electrode array with four laminated layers is 50 μm. In addition, laminated layers with different functions are indispensable. The top and bottom PI layers are packaging layers that aim to prevent environmental interference. The intermediate compartment PI layer prevents signal crosstalk between different layers. The thickness of each layer should be >10 μm; otherwise, it is prone to crosstalk between different layers.

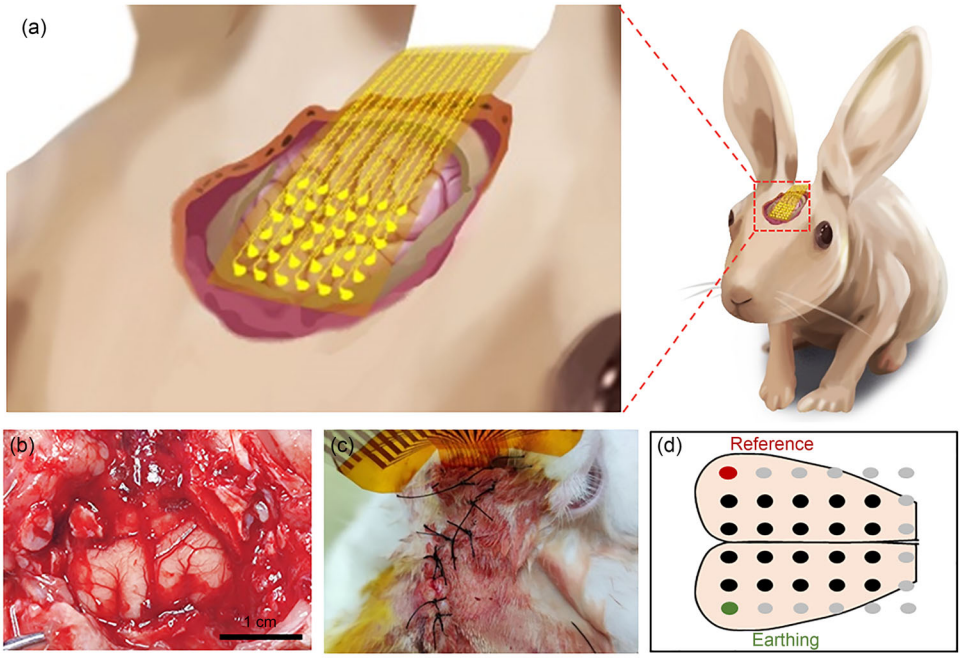

Fig. 4 **a** Schematic diagram of rabbit ECoG acquisition. **b** Rabbit cerebral cortex. **c** Flexible, high-density, laminated ECoG electrode implanted into the rabbit cerebral cortex. **d** Spatial location of electrodes in the rabbit brain. ECoG: electrocorticogram

The conformal ECoG array was placed on the rabbit cortex to collect the neural activity at the location of each electrode. First, the clear rabbit brain cortex was exposed by opening the rabbit skull. In Fig. 4a, the flexible, high-density, laminated ECoG electrode array was attached to the rabbit parietal cortex. Its diameter was about 1 to 1.5 cm (Fig. 4b), consistent with the size of the electrode array. The electrodes were placed on the rabbit brain cortex, and the epidermis was sutured to ensure the stability of ECoG signal acquisition (Fig. 4c and Fig. S4 in Supplementary Information). There are 20 electrodes selected as working electrodes in the flexible, high-density, laminated ECoG electrode array and a reference and a ground electrode outside the active area (Fig. 4d). One 32-channel recording system (customized system; hardware bandpass filter 0.5–100 Hz; sampled at 1000 Hz) was used for recording. Data were analyzed offline using MATLAB. First, each channel signal was bandpass filtered (0.5–100 Hz) and notch filtered at 50 and 100 Hz. Then, the common average reference was used to re-reference the ECoG signal.

Both preinjection and postinjection penicillin ECoGs were recorded in rabbits, which included 20 channels in the analysis. In Fig. S5 (Supplementary Information), cortical ECoG signals were recorded in the rabbit cortex before penicillin injection. The rabbit was anesthetized. ECoG waveforms to be processed were averaged to obtain the average result of the Fourier transform. The cortical ECoG signal was stable, and obvious α-wave signal characteristics were observed (Fig. S5c in Supplementary Information). An α-wave signal was observed in each electrode channel over the whole ECoG acquisition time range. When the α-wave appeared, the rabbit's consciousness was clear, but the body was relaxed, indicating that α waves (approximately 10 Hz) are characteristic cross-species signals, including human and rabbit signals, which provide a "bridge" between the conscious and subconscious.

After penicillin injection, an epileptic wave was induced in rabbits. The flexible, high-density, laminated ECoG electrode array recorded an ECoG signal with 400 s (Fig. 5a). ECoG recordings from the rabbit cerebral cortex revealed high-quality signals, including rapid depolarization of ECoG and the associated spike-wave complex. Spike waves can be seen from the local amplified signal (60–140 s). The amplitude of the spike wave was much larger than that of the common ECoG signal (about 1 to 2 mV; Fig. 5b). The averaged results of the Fourier transform are shown in Fig. 5c. The α wave (approximately 10 Hz) disappeared and the β wave (20–30 Hz) appeared, indicating that the rabbit was in a state of tension. Meanwhile, the signal intensities collected by different electrodes were different, caused by different distances between the electrode and the epilepsy focus (Fig. 5d). ECoG waveforms in the β range (i.e., 20–30 Hz) and >30 Hz often increased after penicillin injection. In Fig. 5e, the *x*-axis represents time, and the *y*-axis represents frequency. Each epileptic activity of rabbits will generate neuroelectric signals with a wide frequency range, corresponding to a red vertical stripe (10–50 Hz) in the spectrum.

Physiologic electrical signals gradually decay with propagation distance. Therefore, the obtained signal intensity is highly correlated with the location of the signal source. The amplitude of the epileptic wave is greater at the position closer to the epilepsy focus. Therefore, the epileptic focus can be located by the energy of the epileptic wave. The spike-wave component captured during the experiment

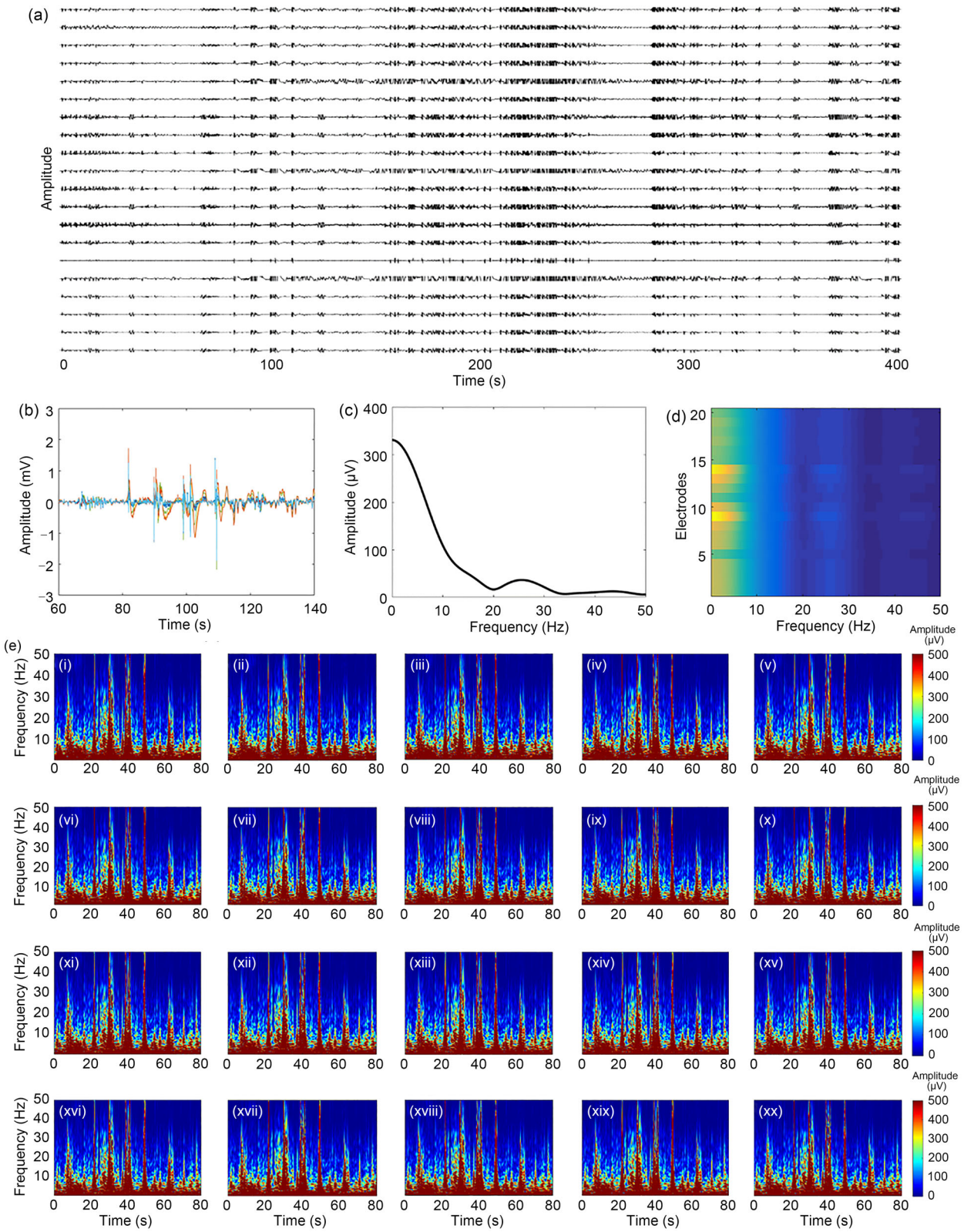

Fig. 5 **a** Rabbit ECoG in the resting state after penicillin injection. **b** Magnified signal view in the range of 60 to 140 s. **c** Fourier transform results of the mean value in the 60 to 140 s range. **d** Color-coded values of Fourier transform results of each channel. **e** Time–frequency analysis results of each channel. ECoG: electrocorticogram

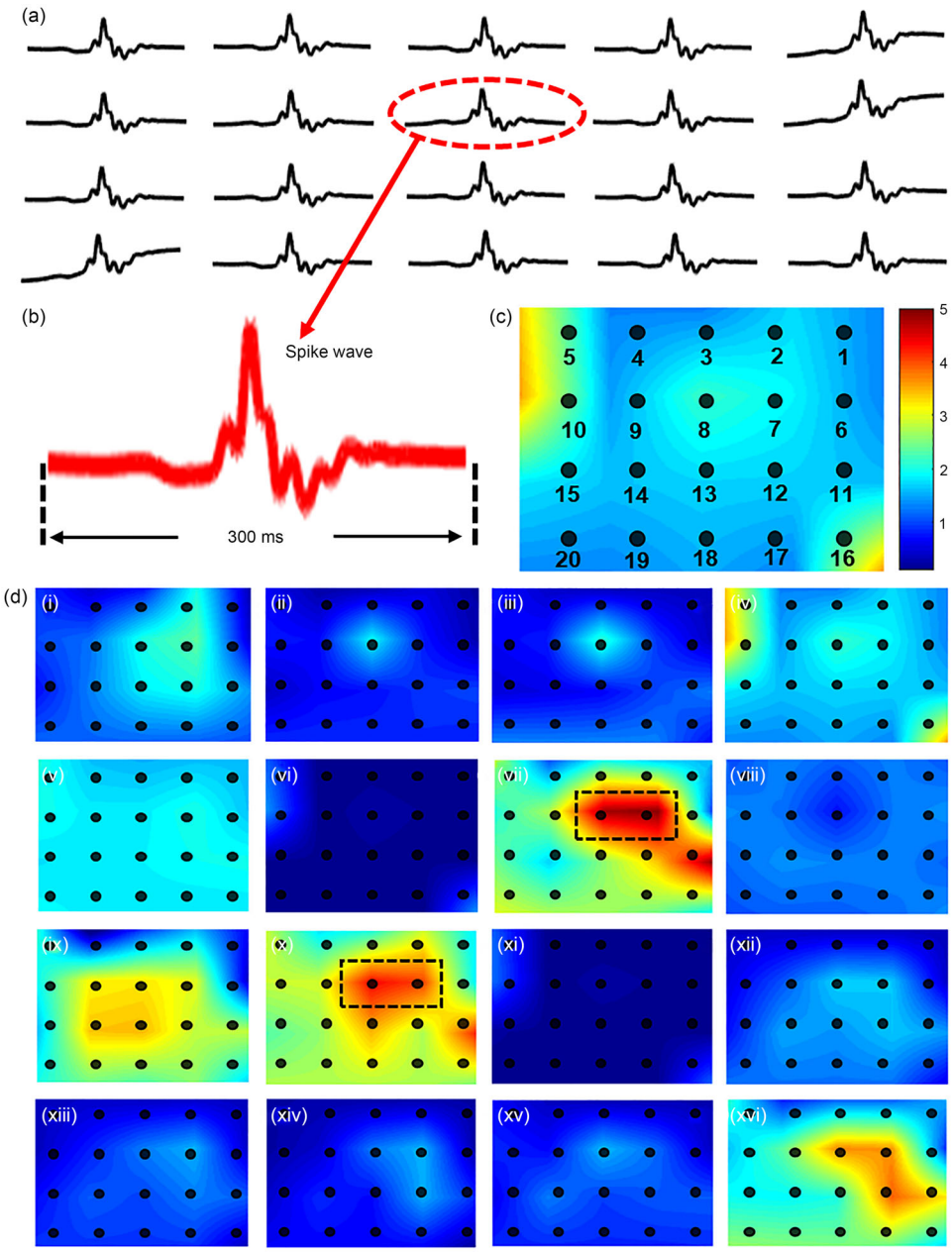

Fig. 6 **a** Representative spike wave in 80 s of rabbit ECoG. **b** Magnified signal view of the spike wave at contact 8. **c** Energy distribution map of rabbit ECoG in 80 s. **d** Energy distribution map of rabbit ECoG at different time subperiods. ECoG: electrocorticogram

of penicillin-induced epilepsy is shown in Fig. 6a. Significant large-scale cortical spikes induced by penicillin can be observed. The duration of a single spike wave is approximately 50 ms (Fig. 6b), consistent with the usual spike signal. By converting the voltage value of the epileptic wave into pseudocolor, the energy distribution map (square of the maximum voltage value) of the epileptic wave is drawn (Fig. 6c). The whole period of 400 s is divided into 16 subperiods, and the energy distribution of different subperiods is illustrated (Fig. 6d). The intensity and distribution of EEG energy change with time. In Fig. 6d, the energy of the seventh (150–175 s) and 10th (225–250 s) subperiods is higher than that of the other subperiods. In the seventh subperiod, the relative energy of channels 7 and 8 is relatively high. In the 10th subperiod, the relative energy of channels 7 and 8 is also relatively high, indicating that electrodes 7 and 8 are closer to the epileptic focus of penicillin-kindled convulsing rabbits. At the same time, the relative energy of electrodes 7 and 8 is relatively high in other subperiods with lower energy. The area corresponding to electrodes 7 and 8 is the epileptic activity area of penicillin-kindled convulsing rabbits.

Traditional ECoG electrodes typically have a diameter of approximately 4 mm and an interelectrode distance of approximately 10 mm. About 40% to 50% of patients have poor surgical outcomes, which is caused by the inaccurate localization of the epileptic focus due to the electrode size

of standard ECoG electrodes being too large. This study reported a class of flexible, ultrathin, high-density ECoG electrode arrays. The challenge of a large number of wiring arrangements was overcome by a laminated structure design and processing technology improvement. Two types of flexible high-density electrodes were prepared by the laminated structure. In focal epilepsy surgery, the flexible, high-density, laminated ECoG electrode array with 36 electrodes was applied to collect epileptic spike waves in rabbits, which verified the feasibility of the laminated structure design. The active area of epilepsy was 2.5 mm long and 1.5 mm wide, which improved the positioning accuracy of epilepsy lesions from the centimeter to the submillimeter level.

Conclusions

This study reported a class of flexible, high-density, laminated ECoG electrode arrays that reliably and robustly enable large-area high-resolution electrophysiologic recordings. First, this study proposed a method of fabricating ultrathin, high-density ECoG electrode arrays with a laminated structure by overlay lithography to achieve high-resolution ECoG acquisition. The laminated structure design enabled the electrode leads to be located in different spatial positions. Importantly, the challenges of a large number of wiring arrangements and the related manufacturing technology of high-density flexible ECoG electrodes with 4444 electrodes per mm^2 were addressed. The minimum spacing between electrodes was 15 μm, comparable to the diameter of a single neuron. In the preparation process, a tempering process was introduced to eliminate the residual thermal stress inside the laminated film structure and overcome the cracking problem of flexible, high-density, laminated ECoG electrodes. The density of the flexible, high-density ECoG electrode was further increased by the laminated structure if necessary. The impedance magnitude at 1 kHz of the flexible laminated ECoG electrode with 36 electrodes was only 6.5 kΩ after bending. In the clinical application of focal epilepsy surgery, the flexible, ultrathin, high-density ECoG electrode introduced in this study can realize the submillimeter-level high-resolution positioning of epileptic lesions and has potential clinical applications in intractable epilepsy and other neurologic diseases requiring high-precision EEG acquisition.

Experimental section

Fabrication of flexible, high-density, laminated ECoG electrodes

Flexible, high-density, laminated ECoG electrodes consisted of four parts: a PI cover, laminated aligned electrodes, a dielectric layer, and a PI base. In the first step, PMMA (M130002, USA), used as a sacrificial layer, was spin-coated on a silicon wafer (3500 r/min, 30 s; 180 °C, 20 min). In the second step, PI (ZKPI-305IIB, POME, China) was spin-coated on the wafer (5000 r/min, 60 s; 80 °C, 15 min; 120 °C, 25 min; 150 °C, 30 min; 180 °C, 30 min; 220 °C, 30 min; 250 °C, 1 h). The prefabricated sample was cooled naturally to room temperature. The sample was heated slowly (1 h) to 250 °C and maintained for 1 h. In the third step, the layers of Cr/Au (10 nm /100 nm) were deposited onto the PI film surface by electron beam evaporation (approximately 0.1 nm/s) and photolithographed into a pattern array. In the fourth step, the dielectric layer was fabricated by spin-coating PI over the designed mesh patterns. The curing temperature and steps of PI were the same as before. Steps 2 to 4 were repeated, and the electrodes were staggered in space. The front and back sides of the multilayer PI/Au film were etched to the electrode shape (circle dot) and connector pad shape (rectangle), respectively, by reactive ion etching masked by Cu (power, 80 W; pressure, 33 Pa; O_2, 30 mL/min).

In vivo animal experiments

The flexible, high-density, laminated ECoG electrode array was placed over the rabbit cortex to record neural activity. First, the clear rabbit cortex was exposed by opening the rabbit skull. The flexible, high-density, laminated ECoG electrode array was attached to the rabbit parietal cortex, and the epidermis was sutured to ensure the stability of ECoG signal acquisition. There were 20 electrodes selected as working electrodes in the flexible, high-density, laminated ECoG electrode array. Both preinjection and postinjection penicillin (cortical parietal lobe, $(0.4461 \pm 0.2549) \times 10^4$ U/kg) ECoGs in rabbits were recorded. The system was a 32-channel recording system (customized system; hardware bandpass filter 0.5–100 Hz; sampled at 1000 Hz). Craniotomy and epileptic wave collection of rabbits were conducted by Beijing Medical Services Biotechnology Co., Ltd. (Beijing, China).

Characterization

Electrochemical experiments of the flexible, high-density, laminated ECoG electrode array were performed on an electrochemical workstation (CS350 type; Corr Test Instruments, China). Electrochemical impedance spectroscopy experiments were carried out by a conventional three-electrode setup (frequency range 0.1–10 kHz, sine-wave amplitude 10 mV, PBS pH 7.2–7.4, temperature approximately 20 °C). The charge injection ability of the electrode was tested by cyclic voltammetry (−0.5 to +0.5 V, 50 mV/s). Flexible, high-density, laminated ECoG electrodes were performed in

two states, i.e., the initial flat and bending states. The bending radius was 5 mm.

Supplementary Information The online version contains supplementary material available at https://doi.org/10.1007/s42242-024-00278-2.

Acknowledgements The authors are grateful for the financial support of the National Natural Science Foundation of China (Nos. U20A6001, 12002190, 11972207, and 11921002), the Fundamental Research Funds for the Central Universities, China (No. SWU-KQ22029), and the Chongqing Natural Science Foundation of China (No. CSTB2022NSCQ-MSX1635).

Author contributions YFL collected the literature and wrote the manuscript. YFL, ZHW, YJ, YC, and GYX prepared the scientific illustrations and experiment data. YFL, YJM, and XF proofread and finalized the revised manuscript. YFL, YJM, and XF conceived the manuscript, prepared, and approved the final version of the manuscript.

Declarations

Conflict of interest The authors declare that they have no conflict of interest.

Ethical approval All institutional and national guidelines for the care and use of laboratory animals were followed. In vivo experiments were conducted in accordance with the Chinese Animal Experimentation Law and approved by the Ethics Committee of Beijing Medical Services Biotechnology (ethical number: MDSW-2021-010C).

References

1. Branco MP, Freudenburg ZV, Aarnoutse EJ et al (2017) Decoding hand gestures from primary somatosensory cortex using high-density ECoG. Neuroimage 147:130–142. https://doi.org/10.1016/j.neuroimage.2016.12.004
2. Choi H, Lee J, Park J et al (2018) Improved prediction of bimanual movements by a two-staged (effector-then-trajectory) decoder with epidural ECoG in nonhuman primates. J Neur Eng 15(1):016011. https://doi.org/10.1088/1741-2552/aa8a83
3. Ryvlin P, Cross JH, Rheims S (2014) Epilepsy surgery in children and adults. Lancet Neurol 13(11):1114–1126. https://doi.org/10.1016/S1474-4422(14)70156-5
4. Jette N, Reid AY, Wiebe S (2014) Surgical management of epilepsy. CMAJ 186(13):997–1004. https://doi.org/10.1503/cmaj.121291
5. Jiruska P, Alvarado-Rojas C, Schevon CA et al (2017) Update on the mechanisms and roles of high-frequency oscillations in seizures and epileptic disorders. Epilepsia 58(8):1330–1339. https://doi.org/10.1111/epi.13830
6. Schalk G, Leuthardt EC (2011) Brain-computer interfaces using electrocorticographic signals. IEEE Rev Biomed Eng 4:140–154. https://doi.org/10.1109/RBME.2011.2172408
7. Chestek CA, Gilja V, Blabe CH et al (2013) Hand posture classification using electrocorticography signals in the gamma band over human sensorimotor brain areas. J Neur Eng 10(2):026002. https://doi.org/10.1088/1741-2560/10/2/026002
8. Wang PT, King CE, McCrimmon CM et al (2016) Comparison of decoding resolution of standard and high-density electrocorticogram electrodes. J Neur Eng 13(2):026016. https://doi.org/10.1088/1741-2560/13/2/026016
9. Siero JCW, Hermes D, Hoogduin H et al (2014) BOLD matches neuronal activity at the mm scale: a combined 7T fMRI and ECoG study in human sensorimotor cortex. NeuroImage 101:177–184. https://doi.org/10.1016/j.neuroimage.2014.07.002
10. Kaiju T, Doi K, Yokota M et al (2017) High spatiotemporal resolution ECoG recording of somatosensory evoked potentials with flexible micro-electrode arrays. Front Neur Circ 11:00020. https://doi.org/10.3389/fncir.2017.00020
11. Thomschewski A, Hincapie AS, Frauscher B (2019) Localization of the epileptogenic zone using high frequency oscillations. Front Neurol 10:00094. https://doi.org/10.3389/fneur.2019.00094
12. Burnos S, Fedele T, Schmid O et al (2016) Detectability of the somatosensory evoked high frequency oscillation (HFO) co-recorded by scalp EEG and ECoG under propofol. Neuroimage Clin 10(C):318–325. https://doi.org/10.1016/j.nicl.2015.11.018
13. Annecchino LA, Schultz SR (2018) Progress in automating patch clamp cellular physiology. Brain Neurosci Adv 2:1–16 https://doi.org/10.1177/2398212818776561
14. Polikov VS, Tresco PA, Reichert WM (2005) Response of brain tissue to chronically implanted neural electrodes. J Neurosci Methods 148(1):1–18. https://doi.org/10.1016/j.jneumeth.2005.08.015
15. Kim DH, Lu NS, Ma R et al (2011) Epidermal electronics. Science 333(6044):838–843. https://doi.org/10.1126/science.1206157
16. Rogers JA, Someya T, Huang YG (2010) Materials and mechanics for stretchable electronics. Science 327(5973):1603–1607. https://doi.org/10.1126/science.1182383
17. Ma YJ, Zhang YC, Cai SS et al (2020) Flexible hybrid electronics for digital healthcare. Adv Mater 32(15):e1902062. https://doi.org/10.1002/adma.201902062
18. Liang ZW, Cheng JH, Zhao Q et al (2019) High-performance flexible tactile sensor enabling intelligent haptic perception for a soft prosthetic hand. Adv Mater Technol 4(8):1900317. https://doi.org/10.1002/admt.201900317
19. Cho Y, Park S, Lee J et al (2021) Emerging materials and technologies with applications in flexible Neur implants: a comprehensive review of current issues with neural devices. Adv Mater 33(47):e2005786. https://doi.org/10.1002/adma.202005786
20. Lang RJ, Tolman KA, Crampton EB et al (2018) A review of thickness-accommodation techniques in origami-inspired engineering. Appl Mech Rev 70(1):010805. https://doi.org/10.1115/1.4039314
21. Marsden AL, Esmaily-Moghadam M (2015) Multiscale modeling of cardiovascular flows for clinical decision support. Appl Mech Rev 67(3):030804. https://doi.org/10.1115/1.4029909
22. Yang SY, Sharma P (2023) A tutorial on the stability and bifurcation analysis of the electromechanical behaviour of soft materials. Appl Mech Rev 75(4):044801. https://doi.org/10.1115/1.4056303
23. Tian L, Zimmerman B, Akhtar A et al (2019) Large-area MRI-compatible epidermal electronic interfaces for prosthetic control and cognitive monitoring. Nat Biomed Eng 3(3):194–205. https://doi.org/10.1038/s41551-019-0347-x
24. Liu YF, Liu Q, Long JF et al (2020) Bioinspired color-changeable organogel tactile sensor with excellent overall performance. ACS Appl Mater Interfaces 12(44):49866–49875. https://doi.org/10.1021/acsami.0c12811
25. Chen YH, Lu SY, Zhang SS et al (2017) Skin-like biosensor system via electrochemical channels for noninvasive blood glucose monitoring. Sci Adv 3(12):e1701629. https://doi.org/10.1126/sciadv.1701629
26. Du QF, Liu LL, Tang RT et al (2021) High-performance flexible pressure sensor based on controllable hierarchical microstructures by laser scribing for wearable electronics. Adv Mater Technol 6(9):2100122. https://doi.org/10.1002/admt.202100122
27. Nguyen JK, Park DJ, Skousen JL et al (2014) Mechanically-compliant intracortical implants reduce the neuroinflammatory response. J Neur Eng 11(5):056014. https://doi.org/10.1088/1741-2560/11/5/056014

28. Subbaroyan J, Martin DC, Kipke DR (2005) A finite-element model of the mechanical effects of implantable microelectrodes in the cerebral cortex. J Neur Eng 2(4):103–113. https://doi.org/10.1088/1741-2560/2/4/006
29. Xu KD, Li SJ, Dong SR et al (2019) Bioresorbable electrode array for electrophysiological and pressure signal recording in the brain. Adv Healthc Mater 8(15):e1801649. https://doi.org/10.1002/adhm.201801649
30. Park AH, Lee SH, Lee CJ et al (2016) Optogenetic mapping of functional connectivity in freely moving mice via insertable wrapping electrode array beneath the skull. ACS Nano 10(2):2791–2802. https://doi.org/10.1021/acsnano.5b07889
31. Zhang YC, Zheng N, Cao Y et al (2019) Climbing-inspired twining electrodes using shape memory for peripheral nerve stimulation and recording. Sci Adv 5(4):eaaw1066. https://doi.org/10.1126/sciadv.aaw1066
32. Yang LT, Liu Q, Zhang ZL et al (2022) Materials for dry electrodes for the electroencephalography: advances, challenges, perspectives. Adv Mater Technol 7(3):00041. https://doi.org/10.1002/admt.202100612
33. Kellis S, Sorensen L, Darvas F et al (2016) Multi-scale analysis of neural activity in humans: implications for micro-scale electrocorticography. Clin Neurophysiol 127(1):591–601. https://doi.org/10.1016/j.clinph.2015.06.002
34. Viventi J, Kim DH, Vigeland L et al (2011) Flexible, foldable, actively multiplexed, high-density electrode array for mapping brain activity in vivo. Nat Neurosci 14(12):1599–1605. https://doi.org/10.1038/nn.2973
35. Khodagholy D, Gelinas JN, Thesen T et al (2015) NeuroGrid: recording action potentials from the surface of the brain. Nat Neurosci 18(2):310–315. https://doi.org/10.1038/nn.3905
36. Hotson G, McMullen DP, Fifer MS et al (2016) Individual finger control of a modular prosthetic limb using high-density electrocorticography in a human subject. J Neur Eng 13(2):026017. https://doi.org/10.1088/1741-2560/13/2/026017
37. Tchoe Y, Bourhis AM, Cleary DR et al (2022) Human brain mapping with multithousand-channel PtNRGrids resolves spatiotemporal dynamics. Sci Transl Med 14(628):eabj1441. https://doi.org/10.1126/scitranslmed.abj1441
38. Zijlmans M, Worrell GA, Dumpelmann M et al (2017) How to record high-frequency oscillations in epilepsy: a practical guideline. Epilepsia 58(8):1305–1315. https://doi.org/10.1111/epi.13814
39. Freeman WJ, Rogers LJ, Holmes MD et al (2000) Spatial spectral analysis of human electrocorticograms including the alpha and gamma bands. J Neurosci Meth 95(2):111–121. https://doi.org/10.1016/S0165-0270(99)00160-0
40. Muller L, Hamilton LS, Edwards E et al (2016) Spatial resolution dependence on spectral frequency in human speech cortex electrocorticography. J Neur Eng 13(5):056013. https://doi.org/10.1088/1741-2560/13/5/056013
41. Wodlinger B, Degenhart AD, Collinger JL et al (2011) The impact of electrode characteristics on electrocorticography. In: Proceedings of the 33rd Annual International Conference of the IEEE EMBS, p.3083–3086. https://doi.org/10.1109/IEMBS.2011.6090842
42. Cotter D, Mackay D, Landau S et al (2001) Reduced glial cell density and neuronal size in the anterior cingulate cortex in major depressive disorder. Arch Gen Psychiat 58(6):545–553. https://doi.org/10.1001/archpsyc.58.6.545
43. Roeske MJ, Konradi C, Heckers S (2021) Hippocampal volume and hippocampal neuron density, number and size in schizophrenia: a systematic review and meta-analysis of postmortem studies. Mol Psychiat 26(7):3524–3535. https://doi.org/10.1038/s41380-020-0853-y
44. Slutzky MW, Jordan LR, Krieg T et al (2010) Optimal spacing of surface electrode arrays for brain-machine interface applications. J Neur Eng 7(2):26004. https://doi.org/10.1088/1741-2560/7/2/026004
45. Ashoori E, Yin HY, Parsnejad S et al (2018) ECoG electrode array with embedded coupling capacitors for area efficient neural recording. In: Proceeding of IEEE Biomedical Circuits and Systems Conference, p.18328093. https://doi.org/10.1109/BIOCAS.2018.8584815
46. Harrison RR, Charles C (2003) A low-power low-noise CMOS for amplifier neural recording applications. IEEE J Solid-S Circ 38(6):958–965. https://doi.org/10.1109/JSSC.2003.811979
47. Yin HY, Ashoori E, Parsnejad S et al (2019) Microfabricated capacitive electrodes for high channel count ECoG recording. In: Proceeding of 9th International IEEE EMBS Conference on Neural Engineering, p.839–842. https://doi.org/10.1109/NER.2019.8717074
48. Wang C, Wei YC, Sung HK et al (2021) Wafer-scale fabrication and assembly method of multichannel microelectrode arrays for ECoG application. Electronics 10(3):316. https://doi.org/10.3390/electronics10030316
49. Wang X, Gkogkidis CA, Iljina O et al (2017) Mapping the fine structure of cortical activity with different micro-ECoG electrode array geometries. J Neur Eng 14(5):056004. https://doi.org/10.1088/1741-2552/aa785e
50. Fischl B, Dale AM (2000) Measuring the thickness of the human cerebral cortex from magnetic resonance images. Proc Natl Acad Sci USA 97(20):11050–11055. https://doi.org/10.1073/pnas.200033797
51. Guz N, Dokukin M, Kalaparthi V et al (2014) If cell mechanics can be described by elastic modulus: study of different models and probes used in indentation experiments. Biophys J 107(3):564–575. https://doi.org/10.1016/j.bpj.2014.06.033
52. Brückner BR, Janshoff A (2015) Elastic properties of epithelial cells probed by atomic force microscopy. BBA-Mol Cell Res 11:3075–3082. https://doi.org/10.1016/j.bbamcr.2015.07.010